

Optimization of Energy Storage Size and Operation for Renewable-EV Hybrid Energy Systems

Jun Chen

ECE, Oakland University
Rochester, MI 48309, USA
Email: junchen@oakland.edu

Zhaojian Li

ME, Michigan State University
East Lansing, MI 48824, USA
Email: lizhaoj1@egr.msu.edu

Xiang Yin

Shanghai Jiao Tong University
Shanghai 200240, China
Email: yinxiang@sjtu.edu.cn

Abstract—This paper focuses on sizing and operation optimization of hybrid energy systems (HES), which integrate multiple electricity generation units (e.g., nuclear, renewable) and multiple electricity consumption units (e.g., grid, EV charging station, chemical plant) for effective management of variability in renewable generation and grid demand. In particular, the operation optimization considers the optimal charging and discharging profile of energy storage element (ESE) so that the variability of the industrial scale chemical plant is minimized. The receding horizon optimization approach is adopted to solve this operation optimization problem, which is then reformulated into a linearly constrained quadratic programming problem, suitable for running in real-time. The design optimization problem finds the optimal sizes of ESE to balance the variability of the chemical plant and the economic cost of ESE installation. Global optimization technique (e.g., DIRECT) is employed to numerically solve the proposed sizing optimization problem, due to its non-convexity.

I. INTRODUCTION

Hybrid energy systems (HES) that consist of multiple energy generation and consumption units have been extensively studied in literature to enable higher level of renewable energy penetration [1]–[17]. By integrating multiple energy units with different response time scales, HES can be operated under flexible operation schedules to accommodate the variability introduced from renewable generation (such as wind farm and solar power) and modern loads (such as electric vehicles) [3]–[5], [11]. In general, HES can be configured to produce different types of energy outputs such as both thermal and electric energy in combined heat and power (CHP) systems [1], utilize different energy resource to produce electricity [2], [8]–[10], [12], [14], [15], [17], or utilize different energy resource to produce multiple energy outputs [3]–[6], [11].

The optimization problems for HES are investigated in literature. For example, the HES design optimization problem is studied in [18], where the optimal sizes of two key components are computed to achieve optimal production while maintaining minimal variability of process variables. Authors of [19], [20] introduce a systematic approach for the design analysis of HES (without thermal output). In particular, the size of a photovoltaic (PV)-wind HES with battery storage is optimized using different optimization strategies such as simulated annealing, response surface methodology, and OptQuest method. Ref. [21] proposes an optimization method for designing hybrid solar-wind systems employing battery

banks, where the optimum system configurations are calculated to maximize economic benefit, while meeting a certain resiliency constraint (e.g., probability of losing power supply). HES design optimization is also discussed in [22], where the benefits of HES are analyzed to increase renewable penetration and to assure power supply security in a particular region. Similar work can also be found in [23], in which the sizes of different components in a grid-independent hybrid PV-wind power systems are optimized.

The literature on HES operation optimization are reviewed as follows. The receding horizon optimization approach is utilized by [2] to optimize the operation of HES to achieve minimum operating and environmental cost while meeting electricity demand. Ref. [12] formulates the HES operation optimization problem as a model predictive controls (MPC) problem to optimally operate a HES with both PV and diesel generation, while energy storage element (ESE) based control for renewable generation smoothing is discussed in [24]. Operation optimization of distributed energy systems are studied in [15], [25], [26], where multi-objective optimization approach is utilized to minimize energy loss in the grid, total electricity generation cost, and greenhouse gas emissions. Fractional PID control is implemented in [27] to the steam supply control of nuclear plant, and the flexible operation of nuclear power plant is realized by dynamic matrix control in [28]. Finally, the coordination control of multiple nuclear plant in the context of hybrid energy systems is investigated in [29].

In this paper, we consider a grid-connected HES configuration consisting of a baseload generation, a wind farm, an EV charging station, an energy storage element (ESE), and an industrial scale chemical plant (e.g., reverse osmosis [RO] desalination plant). The operation optimization problem considered in this paper is to optimize the ESE charging and discharging profile so that the variability of RO process is minimized. In particular, the receding horizon optimization approach is adopted to solve this operation optimization problem, which is then reformulated into a linearly constrained quadratic programming (QP) problem, suitable for running in real-time. The design optimization problem considers the optimal sizes of ESE that balance the variability of RO process and the economic cost of ESE installation. Global optimization technique (e.g., DIRECT) is employed to numerically solve the proposed sizing optimization problem, due to its non-

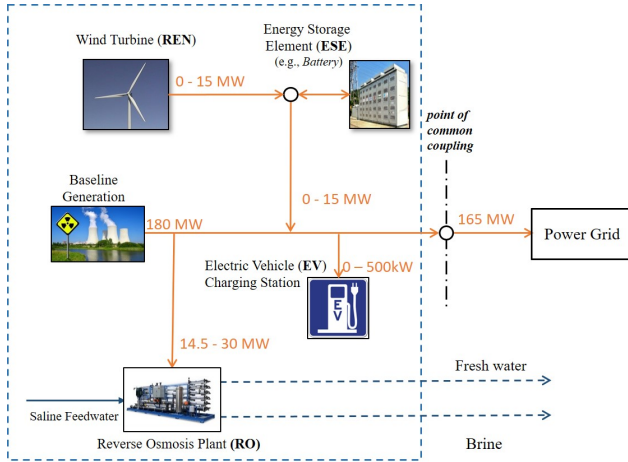


Fig. 1: Topology of the hybrid energy system configuration considered in this paper.

convexity.

The rest of this paper is organized as follows. Section II presents problem formulation including the HES configuration under study. The operation optimization and sizing optimization are detailed in Section III and IV, respectively. Finally, Section V concludes the paper.

II. PROBLEM FORMULATION

A. HES Configuration

The topology of the HES under study is shown within the dotted line in Fig. 1, which includes the following components:

- a baseline electricity generation with 180 MW capacity,
- a series of wind turbines as renewable power generation source with total capacity of 15 MW,
- an energy storage element (e.g., a system scale battery set) used for power smoothing of the electricity generated by wind turbines, whose sizes (maximum charge/discharge power and maximum energy storage capacity) and operation are to be optimized,
- a reverse osmosis plant converting saline water to potable water by consuming 14.5-30 MW electricity,
- an electric vehicle (EV) charging station consuming electricity between 0 and 500 kW,
- electric grid connected to HES at a point of common coupling and consuming 165 MW electricity .

The wind farm considered in Fig. 1 consists of 10 wind turbines, each rated at 1.5 MW, producing a maximum of 15 MW electricity. The generated power of each wind turbine is modeled as a static mapping function of wind speed. See Fig. 2 for a sample 10-day wind speed and wind power generation. The power consumption of EV charging station is modeled as a random process. See Fig. 3 for a sample one-day power consumption of EV charging station.

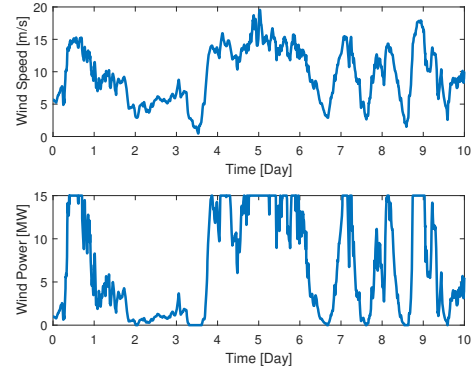


Fig. 2: A sample 10-day wind speed and wind power generation.

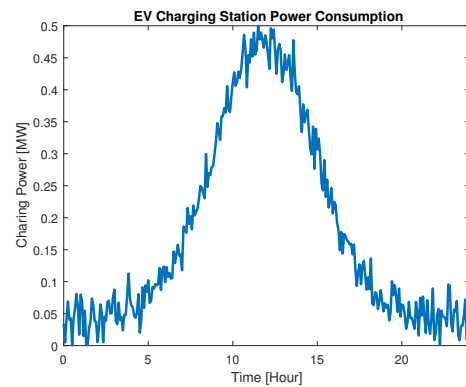


Fig. 3: A sample one-day power consumption of EV charging station.

B. ESE Optimization

Recall that the operation optimization tries to optimize ESE charging and discharging profile, while the sizing optimization tries to find the optimal ESE storage and power configuration. The optimization problem is depicted in Fig. 4, which consists two layers. The inside layer focuses on the operation optimization. Given ESE sizing parameters, the ESE charging/discharging profile is optimized so that the variability of RO plant power consumption is minimized over given wind speed and EV charging profile. The outside layer aims to find the optimal sizes of ESE storage and power so that the RO plant power consumption is minimized. Note that a penalty term is also added in the cost function to penalize large ESE.

III. ESE OPERATION OPTIMIZATION

The HES considered in Fig. 1 is operated such that the baseline is generating constant 180 MW electricity and the HES is delivering 165 MW electricity to power grid. The electricity produced by wind farm and the consumption by EV charging station are variable, and the remaining electricity is consumed by RO. The ESE is operated in a way so that the variability of RO power consumption is minimized.

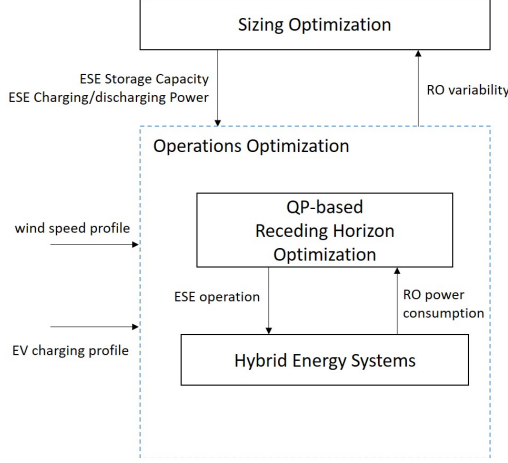


Fig. 4: Two layer optimization for ESE sizing and operation optimization.

A. QP-based Formulation

Denote C_{ESE} as the maximum storage of ESE and P_{ESE} as the maximum charging/discharging power of ESE. The ESE is operated such that its charging/discharging command changes at every discrete time interval ΔT . At given time k and prediction horizon $k+1, \dots, k+N$, where N is the length of prediction horizon, let

- W_0 be the state of charge (SOC) of ESE;
- $P_{RO,0}$ be the current RO power consumption;
- $\hat{P}_{REN} = [\hat{P}_{REN,1}, \dots, \hat{P}_{REN,N}]^T$, be the predicted wind power over prediction horizon;
- $\hat{P}_{EV} = [\hat{P}_{EV,1}, \dots, \hat{P}_{EV,N}]^T$ be the predicted power consumption by EV over prediction horizon;
- finally, $U = [P_{ESE,1}, \dots, P_{ESE,N}]^T$ be the charging or discharge power of ESE over prediction horizon, which are the variables to be computed.

Remark 1: Note that at each time step, the operation optimization problem considered here finds a sequence of N ESE charging/discharging commands over the prediction horizon, but only the first command, i.e., $P_{ESE,1}$ will be implemented and the rest will be disregarded. Then at the next time step, the whole process will be repeated by finding again a sequence of N commands and implementing only the first one. This formulation is called receding horizon optimization [2]. ■

The power consumed by RO over prediction horizon, i.e., $P_{RO} = [P_{RO,0}, \dots, P_{RO,N}]^T$, is given by

$$P_{RO} = 15I_N + \hat{P}_{REN} - \hat{P}_{EV,n} + U,$$

where $I_N = [1, \dots, 1]^T$ has length of N . Note that we adopt the convention that $P_{ESE,n} > 0$ denotes the ESE is discharging and $P_{ESE,n} < 0$ means charging. Hence the variation of $P_{RO,n}$, $n = 0, \dots, N$, is given by

$$J = \frac{1}{N} \sum_{n=1}^N (P_{RO,n} - P_{RO,n-1})^2$$

Note that $P_{RO,0}$, being the current RO power consumption, is a constant. Denote D as a $N \times N$ difference matrix, as follows

$$D = \begin{bmatrix} 1 & 0 & 0 & \cdots & 0 & 0 \\ -1 & 1 & 0 & \cdots & 0 & 0 \\ 0 & -1 & 1 & \cdots & 0 & 0 \\ \vdots & \vdots & \vdots & \ddots & \vdots & \vdots \\ 0 & 0 & 0 & \cdots & -1 & 1 \end{bmatrix}$$

and denote $P_0 = [P_{RO,0}, 0, \dots, 0]^T$ and $C = D(15I_N + \hat{P}_{REN} - \hat{P}_{EV,n}) - P_0$, then we have

$$\begin{aligned} J &= \frac{1}{N} (DP_{RO} - P_0)^T (DP_{RO} - P_0) \\ &= \frac{1}{N} \left(D(15I_N + \hat{P}_{REN} - \hat{P}_{EV,n} + U) - P_0 \right)^T \\ &\quad \times \left(D(15I_N + \hat{P}_{REN} - \hat{P}_{EV,n} + U) - P_0 \right) \\ &= \frac{1}{N} (DU + C)^T (DU + C) \\ &= \frac{1}{N} (U^T D^T D U + 2C^T D U + C^T C) \end{aligned}$$

Ignoring the term in J that are independent on U , we get

$$J = \frac{1}{N} (U^T D^T D U + 2C^T D U) \quad (1)$$

The constraints are formulated as follows. For each $n \in \{0, \dots, N\}$, the charging/discharging power cannot exceed its capacity, and so

$$-P_{ESE}I_N \leq U \leq P_{ESE}I_N \quad (2)$$

Furthermore, the SOC cannot be higher or less than a preset limits, i.e.,

$$w_{lb} \leq W_0 - \sum_{k=1}^n P_{ESE,k} \leq w_{ub}, \forall n \in \{0, \dots, N\}$$

In this paper, we consider $w_{lb} = 1.5$ MWh, which is sufficient for EV charging station to operate at its full capacity for 3 hours, and $w_{ub} = 0.9C_{ESE}$, i.e., the SOC cannot exceed 90% of its maximum storage capacity. Denote S as a $N \times N$ summation matrix, as follows

$$S = \begin{bmatrix} 1 & 0 & 0 & \cdots & 0 & 0 \\ 1 & 1 & 0 & \cdots & 0 & 0 \\ 1 & 1 & 1 & \cdots & 0 & 0 \\ \vdots & \vdots & \vdots & \ddots & \vdots & \vdots \\ 1 & 1 & 1 & \cdots & 1 & 1 \end{bmatrix}$$

Then the above constraint can be rephrased as

$$1.5 \times I_N \leq W_0 I_N - S \Delta T U \leq 0.9 C_{ESE} I_N$$

or equivalently,

$$W_0 I_N - 0.9 C_{ESE} I_N \leq S \Delta T U \leq W_0 I_N - 1.5 I_N \quad (3)$$

Finally, for each $n \in \{1, \dots, N\}$, the power consumed by RO cannot exceed its operating range, i.e.,

$$14.5 I_N \leq P_{RO} = 15 I_N + \hat{P}_{REN} - \hat{P}_{EV,n} + U \leq 30 I_N$$

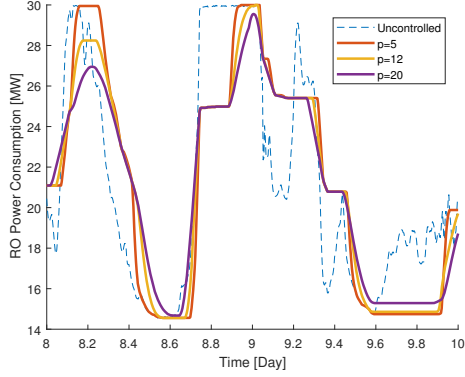


Fig. 5: RO power consumption with respect to time for a 2-day period.

or equivalently,

$$-(0.5I_N + \hat{P}_{REN} - \hat{P}_{EV,n}) \leq U \leq 15I_N - (\hat{P}_{REN} - \hat{P}_{EV,n}) \quad (4)$$

Then the operation optimization problem is formulated as the following QP problem

$$\begin{aligned} \min \quad & J = (1) \\ \text{subject to} \quad & (2), (3) \text{ and } (4) \end{aligned}$$

The QP problem can be solved by active set approach [30], [31], Newton's method [32], or interior point [33], [34]. In this paper, the Matlab's implementation "quadprog" [35] is employed.

B. Numerical Results

The operation optimization problem formulated above was simulated for a 10-day period, with $C_{ESE} = 30$ MWh and $P_{ESE} = 5$ MW. Fig. 5 shows the RO power consumption for a 2-day period, with different prediction horizon N , assuming perfect prediction on wind power generation and EV charging station consumption. The dotted line represents the RO power consumption if no ESE is employed. As can be seen, longer prediction horizon seems to result in a smoother RO operation.

Fig. 6 plots the mean RO ramping rate and the frequency of ESE at maximum charging/discharging power, both with respect to prediction horizon. As can be seen, with longer prediction horizon, the mean ramping rate of RO decreases, aligned with previous results. Similarly, the frequency of ESE utilizing its maximum charging/discharging power also decreases when prediction horizon is extended, hence relaxing the need to have a large ESE.

The results for $N = 12$ are shown in Fig. 7-9. In particular, Fig. 7 shows the ESE charging/discharging power and storage with respect to time. Note that a snapshot of the corresponding RO power consumption was shown in Fig. 5 already. The histogram of ESE charging and discharging power is given in Fig. 8, while the histogram of ESE storage is shown in Fig. 9. As can be seen, most of the time, ESE is operated with moderate charging/discharging behavior (less than 2 MW

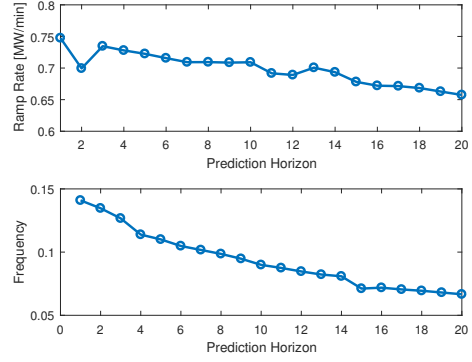


Fig. 6: *Top*: Mean RO ramping rate with respect to prediction horizon; *Bottom*: Frequency of ESE at maximum charging/discharging power with respect to prediction horizon.

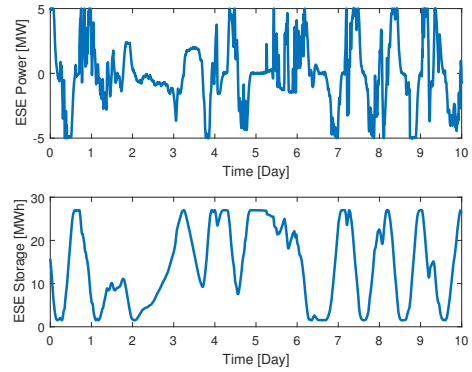


Fig. 7: *Top*: ESE charging/discharging power with respect to time; *Bottom*: ESE storage with respect to time.

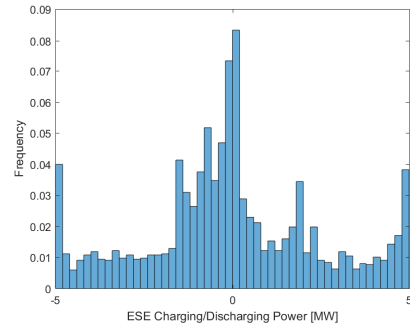


Fig. 8: Histogram of ESE charging and discharging power during 10-day period.

power), and hits the maximum power whenever needed (due to the stochastic nature of wind farm and EV charging station). For almost a quarter of the time, ESE SOC is at the preset upper and lower limit, and is evenly distributed across storage range for the rest of the time.

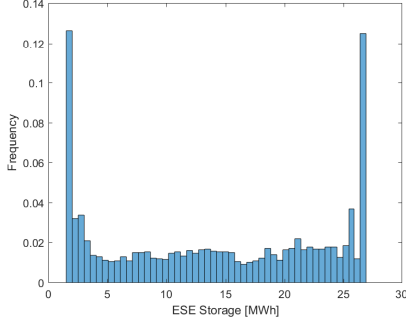


Fig. 9: Histogram of ESE storage during 10-day period.

IV. ESE SIZING OPTIMIZATION

This section discusses the ESE sizing optimization that aims at finding the optimal sizes of ESE storage and power capacity to balance the variability of RO plant as well as the ESE installation cost. Specifically, the following optimization problem is considered,

$$\min J = \lambda_C C_{ESE} + \lambda_P P_{ESE} + \sigma_{RO} \quad (5a)$$

$$\text{subject to} \quad C_{lb} \leq C_{ESE} \leq C_{ub} \quad (5b)$$

where σ_{RO} denotes the variation of RO power consumption and the regularization parameters $\lambda_C > 0$ and $\lambda_P > 0$ penalize large ESE. The lower bound C_{lb} and upper bound C_{ub} ensures the boundedness of the optimization problem. For numerical analysis, they are selected to also ensures the feasibility of the operation optimization problem discussed in previous section. In particular, $C_{lb} = 2$ MWh and $C_{ub} = 50$ MWh are used for numerical simulation presented here.

In order to gain sufficient insights on the optimization problem (5), we simulate the operation optimization for different level of C_{ESE} and P_{ESE} , all with $N = 12$, and plot the RO power consumption as in Fig. 10 and 11. In particular, Fig. 10 plots the RO power consumption against time, for different level of C_{ESE} and P_{ESE} . It appears that as the ESE storage and charging/discharging power capacity increase, the time profile of RO power consumption tend to be smoother. However, as shown in Fig. 11, the variation σ_{RO} of RO power consumption (in terms of mean ramp rate) is a non-convex function w.r.t. C_{ESE} and P_{ESE} . Hence global optimization algorithm (e.g., DIRECT [36], [37]) is utilized to obtain numerical results in this section.

Remark 2: Intuitively, larger C_{ESE} and P_{ESE} should provide better smoothing capability, and lead to smaller σ_{RO} . However, this is true only if the operation optimization has infinite prediction horizon, i.e., $N = \infty$, and the prediction is perfect. In this section, we consider $N = 12$, which can lead to non-monotonic behavior as shown in Fig. 11, making the optimization problem (5) non-convex. ■

The proposed sizing optimization problem (5) is then solved using global optimization algorithm, and the results are summarized in Figures (12)–(14), which plot the optimal C_{ESE}

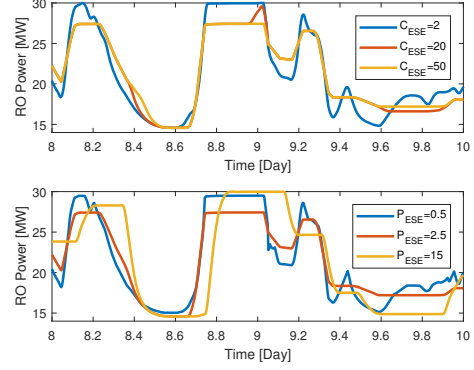


Fig. 10: RO power consumption with respect to time for a 2-day period. *Top:* For different level of C_{ESE} ; *Bottom:* For different level of P_{ESE} .

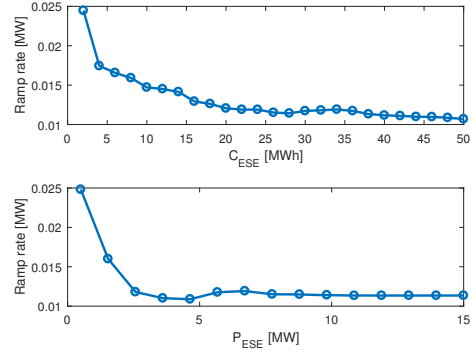


Fig. 11: *Top:* Mean RO ramping rate with respect to C_{ESE} ; *Bottom:* Mean RO ramping rate with respect to P_{ESE} .

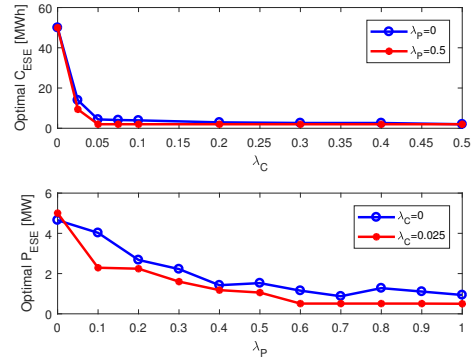


Fig. 12: *Top:* Optimal C_{ESE} with respect to λ_C ; *Bottom:* Optimal P_{ESE} with respect to λ_P .

and P_{ESE} with respect to regulation parameters λ_C and λ_P . In general, when λ_C and λ_P increase, placing a heavier penalty on large ESE, the optimal C_{ESE} and P_{ESE} tend to decrease. This will result in a less smooth RO operation, with the advantage of less capital investment on installing ESE devices.

Remark 3: It should be noted that λ_P and λ_C are hyper-parameters that penalize large ESE, which should be pre-

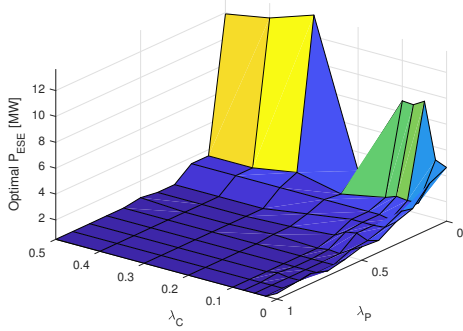


Fig. 13: Optimal P_{ESE} with respect to λ_P and λ_C .

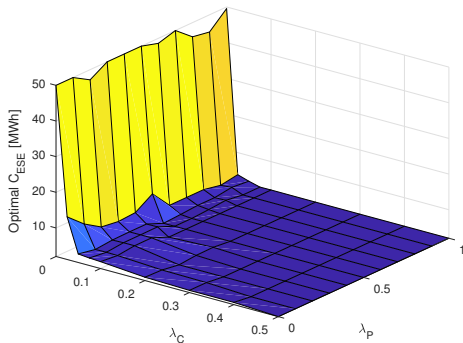


Fig. 14: Optimal C_{ESE} with respect to λ_P and λ_C .

selected to balance the installation cost of ESE and RO variation. It is beyond the scope of this paper to discuss what values of λ_C and λ_P should be selected. However, the methodology presented and discussed in this section, together with the optimization problem formulated in (5), provide a generic framework for HES sizing optimization once λ_C and λ_P are determined. ■

V. CONCLUSION

This paper proposed a framework for sizing and operation optimization for a grid-connected renewable-EV hybrid energy systems. In particular, the operation optimization problem, formulated as a linearly constrained quadratic programming problem, considers the optimal charging and discharging profile of the energy storage elements to minimize the impact of the variability introduced by renewable energy and EV charging station. The design optimization problem finds the optimal sizes of the energy storage element, with regulation terms on penalizing large sizes. Global optimization algorithm is utilized to solve the sizing optimization problem as it is generally non-convex. Future work include (1) analysis of prediction error and its impact on optimization results, (2) scenario based operation optimization with nonlinear battery model [38] and (3) optimization with synthetic data [39] to analyze the sensitivity of the reported results.

ACKNOWLEDGMENT

This work is supported in part by faculty startup fund from School of Engineering and Computer Science at Oakland University.

REFERENCES

- [1] T. Nuytten, B. Claessens, K. Paredis, J. Van Bael, and D. Six, "Flexibility of a combined heat and power system with thermal energy storage for district heating," *Applied Energy*, vol. 104, pp. 583–591, 2013.
- [2] X. Wang, H. Teichgraber, A. Palazoglu, and N. H. El-Farra, "An economic receding horizon optimization approach for energy management in the chlor-alkali process with hybrid renewable energy generation," *J. Process Control*, vol. 24, no. 8, pp. 1318–1327, 2014.
- [3] J. S. Kim, J. Chen, and H. E. Garcia, "Modeling, control, and dynamic performance analysis of a reverse osmosis desalination plant integrated within hybrid energy systems," *Energy*, vol. 112, pp. 52–66, 2016.
- [4] H. E. Garcia, J. Chen, J. S. Kim, R. B. Vilim, W. R. Binder, S. M. B. Sitton, R. D. Boardman, M. G. McKellar, and C. J. Paredis, "Dynamic performance analysis of two regional nuclear hybrid energy systems," *Energy*, vol. 107, pp. 234–258, 2016.
- [5] J. Chen, H. E. Garcia, J. S. Kim, and S. M. Bragg-Sitton, "Operations optimization of nuclear hybrid energy systems," *Nuclear Technology*, vol. 195, no. 2, pp. 143–156, 2016.
- [6] J. Chen and C. Rabiti, "Synthetic wind speed scenarios generation for probabilistic analysis of hybrid energy systems," *Energy*, vol. 120, pp. 507–517, 2017.
- [7] G. Graditi, M. G. Ippolito, E. Telaretti, and G. Zizzo, "An innovative conversion device to the grid interface of combined RES-based generators and electric storage systems," *IEEE Transactions on Industrial Electronics*, vol. 62, no. 4, pp. 2540–2550, 2015.
- [8] J. L. Bernal-Agustín and R. Dufo-López, "Simulation and optimization of stand-alone hybrid renewable energy systems," *Renewable and Sustainable Energy Reviews*, vol. 13, no. 8, pp. 2111–2118, 2009.
- [9] H. Ibrahim, R. Younès, T. Basbous, A. Ilinca, and M. Dimitrova, "Optimization of diesel engine performances for a hybrid wind–diesel system with compressed air energy storage," *Energy*, vol. 36, no. 5, pp. 3079–3091, 2011.
- [10] M. Deshmukh and S. Deshmukh, "Modeling of hybrid renewable energy systems," *Renewable and Sustainable Energy Reviews*, vol. 12, no. 1, pp. 235–249, 2008.
- [11] J. Chen and H. E. Garcia, "Economic optimization of operations for hybrid energy systems under variable markets," *Applied Energy*, vol. 177, pp. 11–24, 2016.
- [12] B. Zhu, H. Tazvinga, and X. Xia, "Switched model predictive control for energy dispatching of a photovoltaic–diesel–battery hybrid power system," *IEEE Trans. Control Syst. Tech.*, vol. 23, no. 3, pp. 1229–1236, May 2015.
- [13] H. Ramadan, M. Becherif, and F. Claude, "Energy management improvement of hybrid electric vehicles via combined gps/rule-based methodology," *IEEE Transactions on Automation Science and Engineering*, vol. 14, no. 2, pp. 586–597, 2017.
- [14] W. Chong, M. Naghavi, S. Poh, T. Mahlia, and K. Pan, "Techno-economic analysis of a wind–solar hybrid renewable energy system with rainwater collection feature for urban high-rise application," *Applied Energy*, vol. 88, no. 11, pp. 4067–4077, 2011.
- [15] G. Graditi, M. L. Di Silvestre, R. Gallea, and E. Riva Sansaverino, "Heuristic-based shiftable loads optimal management in smart microgrids," *IEEE Transactions on Industrial Informatics*, vol. 11, no. 1, pp. 271–280, 2015.
- [16] P. Meibom, R. Barth, B. Hasche, H. Brand, C. Weber, and M. O'Malley, "Stochastic optimization model to study the operational impacts of high wind penetrations in Ireland," *IEEE Trans. Power Syst.*, vol. 26, no. 3, pp. 1367–1379, 2011.
- [17] G. Bekele and B. Palm, "Feasibility study for a standalone solar–wind-based hybrid energy system for application in ethiopia," *Applied Energy*, vol. 87, no. 2, pp. 487–495, 2010.
- [18] W. Du, H. E. Garcia, and C. J. J. Paredis, "An optimization framework for dynamic hybrid energy systems," in *Proc. 10th Int. Modelica Conf.*, Lund, Sweden, Mar. 10–12, 2014, pp. 767–776.
- [19] O. Ekren and B. Y. Ekren, "Size optimization of a pv/wind hybrid energy conversion system with battery storage using simulated annealing," *Applied Energy*, vol. 87, no. 2, pp. 592–598, 2010.

- [20] B. Y. Ekren and O. Ekren, "Simulation based size optimization of a pv/wind hybrid energy conversion system with battery storage under various load and auxiliary energy conditions," *Applied Energy*, vol. 86, no. 9, pp. 1387–1394, 2009.
- [21] H. Yang, Z. Wei, and L. Chengzhi, "Optimal design and techno-economic analysis of a hybrid solar–wind power generation system," *Applied Energy*, vol. 86, no. 2, pp. 163–169, 2009.
- [22] D. A. Hagos, A. Gebremedhin, and B. Zethraeus, "Towards a flexible energy system—a case study for inland norway," *Applied Energy*, vol. 130, pp. 41–50, 2014.
- [23] A. Kaabeche, M. Belhamel, and R. Ibtouen, "Sizing optimization of grid-independent hybrid photovoltaic/wind power generation system," *Energy*, vol. 36, no. 2, pp. 1214–1222, 2011.
- [24] X. Li, D. Hui, and X. Lai, "Battery energy storage station (bess)-based smoothing control of photovoltaic (pv) and wind power generation fluctuations," *IEEE transactions on sustainable energy*, vol. 4, no. 2, pp. 464–473, 2013.
- [25] M. Di Somma, B. Yan, N. Bianco, G. Graditi, P. B. Luh, L. Mongibello, and V. Naso, "Operation optimization of a distributed energy system considering energy costs and exergy efficiency," *Energy Conversion and Management*, vol. 103, pp. 739–751, 2015.
- [26] M. Ippolito, M. Di Silvestre, E. R. Sanseverino, G. Zizzo, and G. Graditi, "Multi-objective optimized management of electrical energy storage systems in an islanded network with renewable energy sources under different design scenarios," *Energy*, vol. 64, pp. 648–662, 2014.
- [27] A. Salehi, O. Safarzadeh, and M. H. Kazemi, "Fractional order pid control of steam generator water level for nuclear steam supply systems," *Nuclear Engineering and Design*, vol. 342, pp. 45–59, 2019.
- [28] D. Jiang and Z. Dong, "Dynamic matrix control for thermal power of multi-modular high temperature gas-cooled reactor plants," *Energy*, p. 117386, 2020.
- [29] Z. Dong, M. Song, X. Huang, Z. Zhang, and Z. Wu, "Coordination control of smr-based nsss modules integrated by feedwater distribution," *IEEE Transactions on Nuclear Science*, vol. 63, no. 5, pp. 2682–2690, 2016.
- [30] G. B. Dantzig, "Quadratic programming. a variant of the wolfe-markowitz algorithms," California Univ Berkeley Operation Research Center, Tech. Rep., 1961.
- [31] D. Goldfarb and A. Idnani, "A numerically stable dual method for solving strictly convex quadratic programs," *Mathematical programming*, vol. 27, no. 1, pp. 1–33, 1983.
- [32] T. F. Coleman and Y. Li, "A reflective newton method for minimizing a quadratic function subject to bounds on some of the variables," *SIAM Journal on Optimization*, vol. 6, no. 4, pp. 1040–1058, 1996.
- [33] J. Nocedal and S. Wright, *Numerical optimization*. Springer Science & Business Media, 2006.
- [34] S. Boyd, S. P. Boyd, and L. Vandenberghe, *Convex optimization*. Cambridge university press, 2004.
- [35] <https://www.mathworks.com/help/optim/ug/quadprog.html>.
- [36] D. R. Jones, C. D. Perttunen, and B. E. Stuckman, "Lipschitzian optimization without the lipschitz constant," *Journal of optimization Theory and Applications*, vol. 79, no. 1, pp. 157–181, 1993.
- [37] D. R. Jones, "Direct global optimization algorithm," *Encyclopedia of optimization*, pp. 431–440, 2001.
- [38] D. Wu, P. Balducci, A. Crawford, V. Viswanathan, and M. Kintner-Meyer, "Optimal control for battery storage using nonlinear models," in *Proc. EESAT Conf*, 2017.
- [39] J. Chen, J. S. Kim, and C. Rabiti, "Probabilistic analysis of hybrid energy systems using synthetic renewable and load data," in *Prof. 2017 American Control Conference*, Seattle, WA, May, 2017, pp. 4723–4728.